

**HYPERMATTER
-PROPERTIES AND FORMATION
IN RELATIVISTIC NUCLEAR COLLISIONS**

L. Gerland, C. Spieles, M. Bleicher, P. Papazoglou, J. Brachmann, A. Dumitru,
H. Stöcker, W. Greiner

*Institut für Theoretische Physik, J.W. Goethe-Universität
D-60054 Frankfurt, Germany*

J. Schaffner

*Niels Bohr Institute, Blegdamsvej 17
DK-2100 Copenhagen, Denmark*

C. Greiner

*Institut für Theoretische Physik, J. Liebig-Universität,
D-35392 Giessen, Germany*

The extension of the Periodic System into hitherto unexplored domains - antimatter and hypermatter - is discussed. Starting from an analysis of hyperon and single hypernuclear properties we investigate the structure of multi-hyperon objects (MEMOs) using an extended relativistic meson field theory. These are contrasted with multi-strange quark states (strangelets). Their production mechanism is studied for relativistic collisions of heavy ions from present day experiments at AGS and SPS to future opportunities at RHIC and LHC. It is pointed out that absolutely stable hypermatter is unlikely to be produced in heavy ion collisions. New attention should be focused on short lived metastable hyperclusters ($\tau \propto 10^{-10}$ s) and on intensity interferometry of multi-strange-baryon correlations.

1 Motivation

Since Mendelejew's and Meyer's discovery of regular patterns in the periodic system of elements (then only 60 elements were known) has the systematic discovery of new elements been a vital motivation for science.

1.1 Extension of the Periodic System and Nuclear Phasediagram

The synthesis of new elements 107 - 111 using the cold fusion method at GSI during the last decade represents milestones on the way to a possible super-heavy island around $Z \approx 114$ ^{1,2}. Fig. 1 shows the chart of nuclei, as of January 1996, with the new elements at the far right end. Exotic isotopes as e.g. ¹⁰⁰Sn, ¹⁵¹Ln, ¹¹Li, discovered at GSI, CAEN, LBL and Riken, are also shown. The magic numbers for protons and neutrons and the proton- and neutron drip

lines are indicated. The crosses (\times) show the large number of newly discovered isotopes, extending the chart of nuclei from the stable valley outwards to the "shallow waters" of the drip lines.

This picture is to big !

Figure 1: The full chart of nuclei

Due to the fermi-energy, nuclei tend to consist of as many protons as neutrons. However, with increasing charge the nuclei become unstable due to the Coulomb-interaction: the chart of nuclei is limited in each direction for nuclei which are "built" of protons and neutrons.

However, here we shall discuss whether it could be possible to extend the chart of nuclei in new domains, using new degrees of freedom, namely strangeness!

Properties of Hyperons

The flavour SU(3) - triplet contains u-, d- and s-quarks. Ordinary matter is solely built of u- and d-quarks. It is therefore an intriguing thought to search for matter with s-quarks, which we shall call **strange matter**, if it contains sufficiently many s-quarks per u- and d-quarks. Fig. 2 shows the quark-content of spin 1/2 nucleons and hyperons contained in the octet and of spin 3/2 baryons contained in the decouplet. Table 1 reviews properties of these baryons.

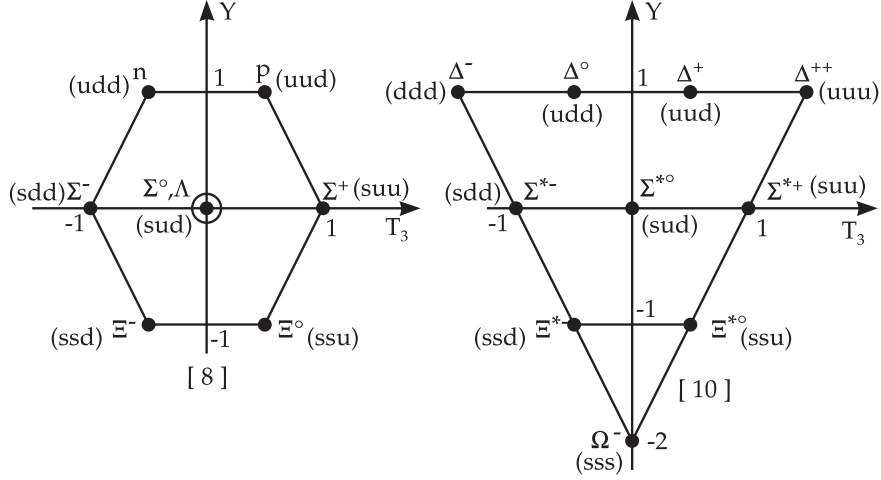


Figure 2: The octet of spin 1/2 nucleons and hyperons (left) and the decuplet of spin 3/2 baryons (right). The quark content of the particles is indicated.

	J^P	T	S[C]	mass[MeV]	lifetime[s]	main decays
p	$1/2^+$	1/2	0	938.27	$> 10^{25}$ years	stable
n	$1/2^+$	1/2	0	939.56	887.0 ± 2.0	$p e^- \bar{\nu}_e$ (100%)
Λ	$1/2^+$	0	-1	1115.7	2.63×10^{-10}	$p\pi^-$ (64.1%), $n\pi^0$ (35.7%)
Σ^+	$1/2^+$	1	-1	1189.4	0.799×10^{-10}	$p\pi^0$ (51.6%), $n\pi^+$ (48.3%)
Σ^0	$1/2^+$	1	-1	1192.6	7.4×10^{-20}	$\Lambda\gamma$ (100%)
Σ^-	$1/2^+$	1	-1	1197.4	1.48×10^{-10}	$n\pi^-$ (99.8%)
Ξ^0	$1/2^+$	1/2	-2	1314.9	2.90×10^{-10}	$\Lambda\pi^0$ (100%)
Ξ^-	$1/2^+$	1/2	-2	1321.3	1.64×10^{-10}	$\Lambda\pi^-$ (100%)
Ω^-	$3/2^+$	0	-3	1672.4	0.82×10^{-10}	ΛK^- (67.8%), $\Xi^- \pi^0$ (8.6%), $\Xi^0 \pi^-$ (23.6%)
Λ_c^+	$1/2^+$	0	0[1]	2285	2.0×10^{-13}	
Ξ_c^+	$1/2^+$	1/2	-1[1]	2466	3.5×10^{-13}	
Ξ_c^0	$1/2^+$	1/2	-1[1]	2470	1.0×10^{-13}	
Λ_b^0	$1/2^+$	0	B=-1	5641	1.1×10^{-12}	

Table 1 : Properties of "stable" baryons and their weak decay modes. J stands for spin, P for parity and T for isospin. The branching ratios of the decays of particles with charm (bottom) are not yet well known. ³

Strange Nuclei

There are various ways to venture from ordinary matter (built out of protons (Z) and neutrons (N) in nuclei with baryon number $A = Z + N$) into the sector of strange matter (Fig. 3).

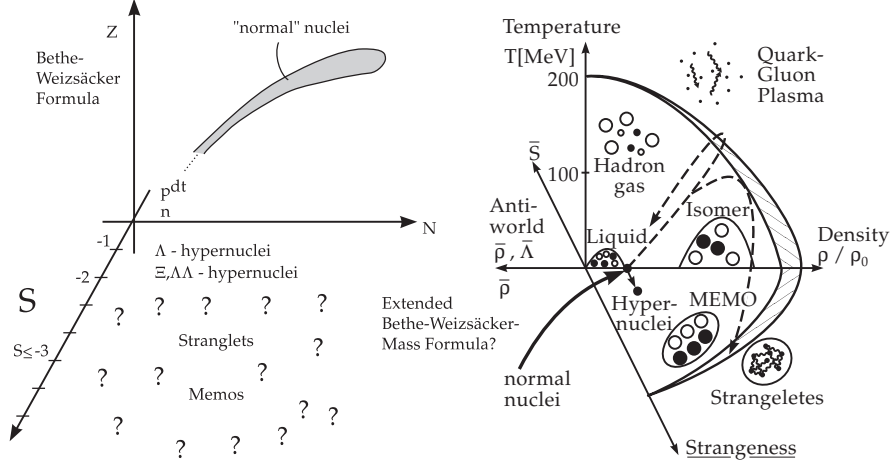


Figure 3: Schematic view of the novel extension of the Periodic System (proton-, Z , and neutron number, N , plane) into the direction of finite net strangeness S

One possibility is to add baryons with strangeness (Λ , Ξ , ...) to ordinary nuclei. However, strange baryons are short lived, therefore adding consecutively strangeness to hypernuclei (e.g. with kaon beams) seems unfeasible. Only in the interior of neutronstars or in relativistic heavy ion collisions one can expect the simultaneous presence and density of sufficiently many hyperons/strange quarks to allow for a search for multi-strange matter. Baryons and mesons in dense matter may also dissolve and form "strangelets" of u -, d -, and s -quarks.

1.2 Heavy Ion Collisions

Relativistic heavy ion collisions are the only tool to probe hot and dense nuclear matter, where one might create such new forms of nuclear matter, i.e. MEMOs (Metastable Exotic Multistrange Object) and strangelets. Fig. 4 shows different paths for nuclear matter in the phase diagram in heavy ion collisions. Starting at the ground state of ordinary nuclear matter, at ρ_0 and $T = 0$,

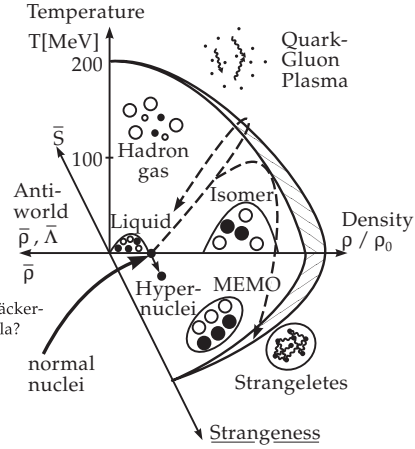


Figure 4: Sketch of the nuclear matter phase diagram

various excursions through that phase diagram are indicated. As a result of such collisions ordinary elementary particles of all kinds are produced. They constitute the "ashes" of what was encountered during the high density state of the reactions.

Can such matter be stable? This question can be studied theoretically by extending well tested models of nuclear structure into the strangeness domain.

2 Stability and Existence of Strange Matter

Here we study the possibilities for extending the chart of nuclei into these new domains by following our knowledge of normal nuclei. We use the Relativistic Mean Field-(RMF)-model which has been applied successfully in numerous applications to normal nuclei. It consists of an effective Meson-Baryon Lagrangean with scalar (σ) and vector (ω, ρ) fields.

2.1 MEMOs - Strange Nuclei

Calculation of Nuclei - RMFT: ^{100}Sn

An example for the successful application of the RMF-model to exotic nuclear states is the prediction of the shell model potential and level structure for the exotic ^{100}Sn -isotope shown in Fig. 5. It reproduces the experimentally measured Q-value of this exotic heaviest $Z = N$ doubly closed shell nucleus.

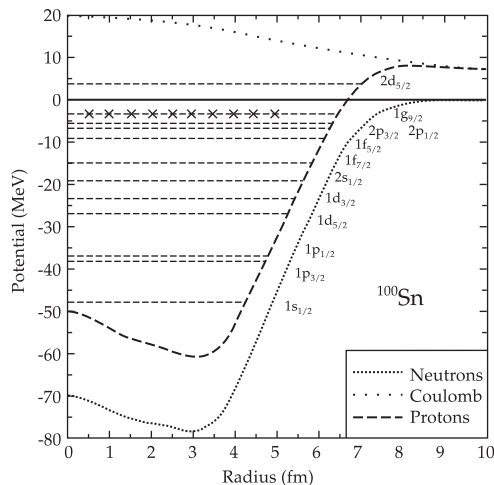


Figure 5: Prediction of the shell model potential and level structure for the exotic ^{100}Sn -isotope. Proton- and neutron potentials are shown ⁴.

Extension of RMFT to Hyperons

This RMF-model has been extended to include single Λ -hypernuclei⁵. Fig. 6 shows the measured single particle energy for different single Λ -hypernuclei in comparison with RMF calculations using only two free parameters, namely the two coupling constants of the Λ ($g_{\sigma\Lambda}$ and $g_{\omega\Lambda}$), which are correlated: they are fixed by the potential depth of the Λ

$$U_{\Lambda} = -g_{\sigma\Lambda}\sigma - g_{\omega\Lambda}V_0 \quad (1)$$

in saturated nuclear matter⁶.

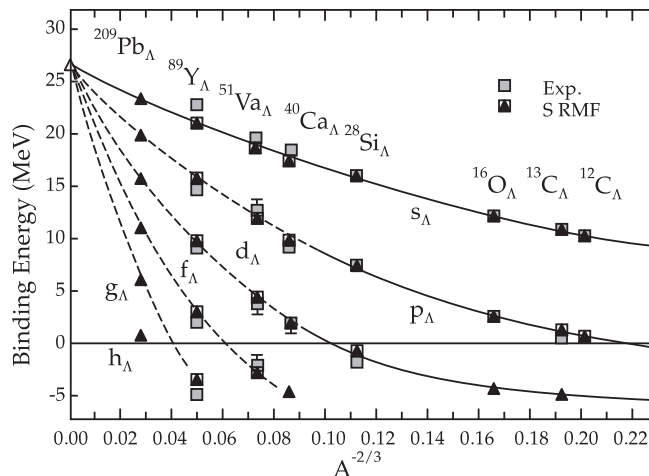


Figure 6: The single particle energy of several hypernuclei⁷ in comparison with RMF calculations.

One can choose for all spin 1/2 baryons, for example, SU(6)-symmetry for the (u,d)-quark content dependent vector coupling constants to the ω -field

$$g_{\omega N} = \frac{3}{2}g_{\omega\Lambda} = \frac{3}{2}g_{\omega\Sigma} = 3g_{\omega\Xi}. \quad (2)$$

The scalar coupling constants can be fitted to the potential depth of the corresponding hyperon.

A χ^2 -fit of the coupling constants to experimental data on single- Λ -hypernuclei is shown in Fig. 7. Note that only **ratios** of $g_{\sigma\Lambda}$ and $g_{\omega\Lambda}$ can be fixed, but there is a considerable uncertainty in fixing just one parameter.

This picture is to big !

Figure 7: χ^2 -Fit of the coupling constants to experimental data on single- Λ -hypernuclei

Typical potentials for Λ 's and nucleons are given in Fig. 8. Obviously the spin-orbit-splitting is much smaller for Λ 's as compared to that of the nucleons. Also the potential is $U_\Lambda \approx 1/2U_N$.

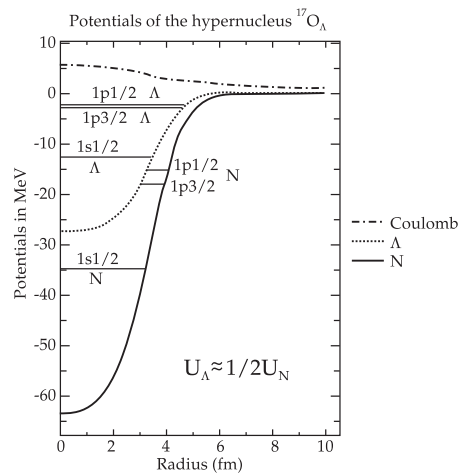


Figure 8: Typical potential wells for the Λ s and for nucleons in case of the hypernucleus ^{17}O . Note that approximately $U_\Lambda \approx 1/2U_N$.

This model 1 reproduces well the properties of single Λ -hypernuclei. However, as we will discuss below, with this model it is not able to reproduce the observed strongly attractive $\Lambda\Lambda$ interaction. (The situation can be remedied^{7,4} by introducing two additional meson fields, the scalar meson $f_0(975)$ (denoted as σ^* in the following) and the vector meson $\phi(1020)$ (model 2).)

Extension to Light Hypernuclei

Now that the coupling constants are determined from experiment, the RMF-model can be tested by *predicting* the properties of light ($A < 16$) single Λ hypernuclei. This serves as a test of the predictive power of the model. Fig. 9 shows the binding energies of such light hypernuclei as measured and as calculated without adjusting any free parameters for the non-spherical nuclei. The prediction are within 10% of the experimental values. This gives confidence into using the model in hitherto unexplored domains of hyperon combinations.

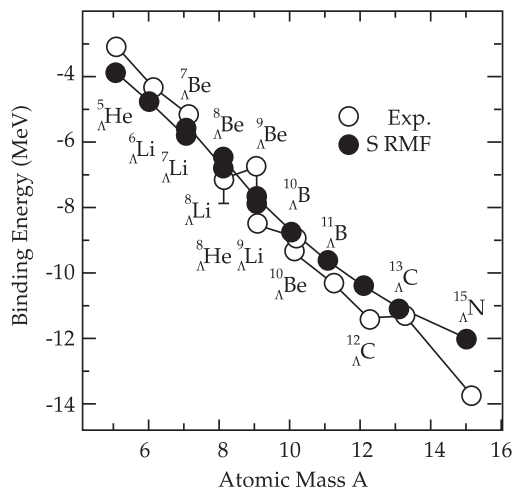


Figure 9: Calculated binding energies for a Λ -particle in a light nucleus. The experiment is shown in open circles (\circ), the theory in full circles (\bullet). The data are from⁸.

$\Lambda\Lambda$ -Interaction

Such an unexplored domain is the study of multihypernuclei. Few data are available for double Λ -nuclei (for a review see⁹). Fig. 11 shows that there is a substantial additional $\Lambda\Lambda$ attraction, not taken care of in the standard RMF-model. This has been implemented (see model 2 below). Fig. 10 shows the

density distribution of the double- Λ hypernucleus ${}^6\text{He}_{\Lambda\Lambda}$. Every baryon sits in its respective $1s_{1/2}$ -state. The Λ -density is indicated by the dashed area. Evidently an enhanced interaction radius results. The lifetime of the Λ 's is of the order $\tau \approx 10^{-10}\text{s}$. This behaviour is that of like the $Z=2$ anomalon.

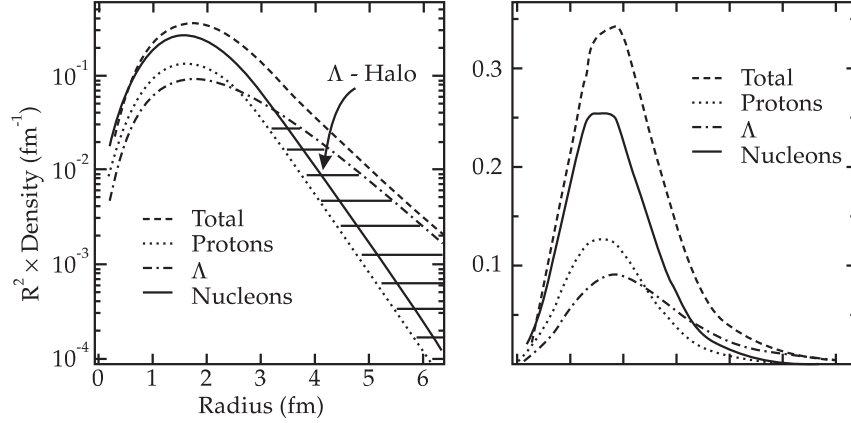


Figure 10: Density distribution of the highly symmetric double- Λ hypernucleus ${}^6\text{He}_{\Lambda\Lambda}$.

However, it turns out that this model underpredicts the measured $\Lambda\Lambda$ -interaction for a Λ -vector-coupling-constant between 0 and g_{vN} [Fig. 11]. Therefore 6 additional $\Lambda\Lambda$ binding must be implemented into the theory. In the Mean Field Approximation this can be done e.g. by adding scalar and vector mesons to the Lagrangean.

The additional Lagrangean then reads

$$\mathcal{L}' = \mathcal{L} + \mathcal{L}_{\text{Meson}}^{YY} + \mathcal{L}_{\text{Coupling}}^{YY}, \quad (3)$$

with

$$\mathcal{L}_{\text{Meson}}^{YY} = \frac{1}{2} \left(\partial_\nu \sigma^* \partial^\nu \sigma^* - m_{\sigma^*}^2 \sigma^{*2} \right) - \frac{1}{4} S_{\mu\nu} S^{\mu\nu} + \frac{1}{2} m_\phi^2 \phi_\mu \phi^\mu, \quad (4)$$

$$\mathcal{L}_{\text{Coupling}}^{YY} = - \sum_B g_{\sigma^* B} \bar{\Psi}_B \Psi_B \sigma^* - \sum_B g_{\phi B} \bar{\Psi}_B \gamma_\mu \Psi_B \phi^\mu. \quad (5)$$

The equations of motion for the additional meson fields read :

$$\begin{aligned} (-\Delta + m_{\sigma^*}^2) \sigma^* &= -g_{\sigma^* \Lambda} \rho_{s\Lambda} - g_{\sigma^* \Sigma} \rho_{s\Sigma} - g_{\sigma^* \Xi} \rho_{s\Xi}, \\ (-\Delta + m_\phi^2) \phi_0 &= +g_{\phi \Lambda} \rho_{v\Lambda} + g_{\phi \Sigma} \rho_{v\Sigma} + g_{\phi \Xi} \rho_{v\Xi}, \end{aligned} \quad (6)$$

with the respective scalar and vector densities. Together with the equations for the σ -, V_0 - and $R_{0,0}$ -meson fields and for the Coulomb field A_0 , all of which are unchanged, coupled system of nonlinear partial differential equations results, which is solved selfconsistently. The coupling constants are fixed by the $SU(6)$ -relations:

$$\frac{g_{\phi\Lambda}}{g_{vN}} = -\frac{\sqrt{2}}{3} \quad , \quad \frac{g_{\phi\Xi}}{g_{vN}} = -\frac{2\sqrt{2}}{3}. \quad (7)$$

The hyperon-hyperon-interaction is fixed to extrapolated depths of the $U_Y^{Y'}$ -potentials⁴.

This extended model 2 is now closer to the experimental value of the $\Lambda\Lambda$ -interaction matrix element (see Fig. 11).

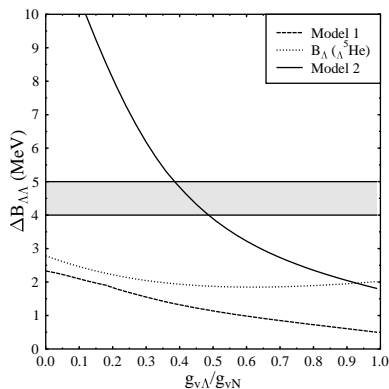


Figure 11: The matrix element $\Delta B_{\Lambda\Lambda}$ as a function of the vector coupling constant of the Λ in model 1 and 2.

Hypermatter – Stable Combinations of several Hyperons

Now that all hyper-data known are described, one can go about extending our chart of nuclei into areas **without any** protons and neutrons! However, keep in mind that strong reactions might change the hyperon-nucleon composition with millibarn crosssections.

All possible metastable combinations of two baryons are listed in table 2 .

$-S \setminus Z$	-2	-1	0	+1	+2
0			nn	np	pp
1		$\Sigma^- n$	Λn	Λp	$\Sigma^+ p$
2	$\Sigma^- \Sigma^-$	$\Xi^- n$	$\Lambda \Lambda$	$\Xi^0 p$	$\Sigma^+ \Sigma^+$
3	$\Xi^- \Sigma^-$	$\Xi^- \Lambda$	$\Xi^0 \Lambda$	$\Xi^0 \Sigma^+$	
4	$\Xi^- \Xi^-$	$\Xi^0 \Xi^-$	$\Xi^0 \Xi^0$		
5	$\Xi^- \Omega^-$	$\Xi^0 \Omega^-$			
6	$\Omega^- \Omega^-$				

Table 2 : Possible metastable doublets of the members of the baryon octet and of the Ω^- .

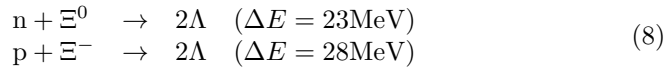
Metastable (i.e. stable with respect to strong interaction) combinations of three different species are listed in table 3 . Of special interest are metastable systems consisting of $\{\Lambda, \Xi^0, \Xi^-\}$ -hyperons: do they form clusters of purely hyperonic matter? More than three different baryon species cannot form a metastable combination in free space, but binding effects can change this statement in clusters of hypermatter.

$-S \setminus Z$	-2	-1	0	+1	+2
1				Λnp	
2					
3	$\Xi^- \Sigma^- n$	$\Xi^- \Lambda n$		$\Xi^0 \Lambda p$	$\Xi^0 \Sigma^+ p$
4					
5		$\Xi^- \Xi^0 \Lambda$			
6					
7	$\Omega^- \Xi^- \Xi^0$				

Table 3 : Metastable triplets of nucleons and hyperons sorted according to strangeness S and charge Z .

MEMOs - Stability due to Pauli Blocking

Let us turn to the structure of bound exotic multi-strange nuclei. They can be formed by adding Σ 's (see^{6,7}) and Ξ 's. The latter may react strongly according to



However, if there are already several Λ 's within the nucleus, these reactions can eventually be Pauli-blocked. The idea is illustrated in the Fig. 12 for the

Superheavy Hypernuclei

Now, even heavier systems can be calculated in the extended RMF-model, their structure and stability can be studied. The binding energy of multi-strange nuclei is plotted in Fig. 14 versus the strangeness fraction $f_s = |S|/A$ for model 1 and model 2 for various nuclear cores. It is interesting to note that the minima of the curves are located around $f_s \approx 0.6$ for model 1 and $f_s \approx 1.0$ for model 2, which is in the same range as for strangelets as discussed below. A striking example for the enhanced stability is the sequence with a ^{180}Th core in model 2. The nuclear core ^{180}Th consisting of 90 protons and 90 neutrons is unstable - it is far beyond the proton drip line. Nevertheless, the addition of strangeness (hyperons) can stabilize the systems and results in binding energies of about $E/A \approx -20$ MeV!

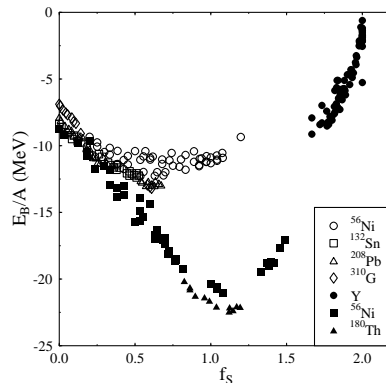


Figure 14: Binding energy versus the strangeness fraction for SHM(strange hadronic matter) in model 1 (nuclear cores ^{56}Ni , ^{132}Sn , ^{208}Pb , ^{310}G) and model 2 (^{56}Ni , ^{180}Th , Y denotes purely hyperonic systems).⁷

Pure Hyperclusters - Neutral and Negatively Charged Nuclei

Figs. 14 and 15 show that in the RMF model exhibits also pure hyperon clusters (denoted as Y). They consist only of $\{\Lambda, \Xi^0, \Xi^-\}$ -hyperons. Their net strangeness fraction is $f_s \approx 1.7$ and the charge fraction is $f_q \approx -0.3$. Pure hyperon clusters are only bound in model 2 due to the implemented hyperon-hyperon interaction). The binding energy per baryon reaches $E/A \approx 3 - 8$ MeV, $f_s \approx 2$, and $f_q \approx -0.4$. Fig. 16 shows the binding energy of MEMOS versus the mass A. Note that E_B/A drops linearly with A. Let us now turn to

the dual counterparts of MEMOs, namely the strangelets.

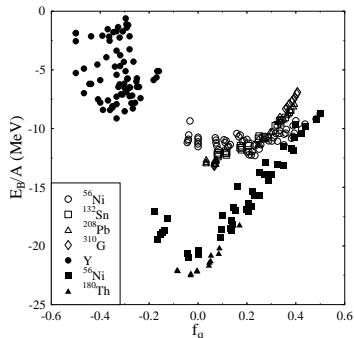


Figure 15: Binding energy per baryon versus the charge fraction f_q for strange hadronic matter.⁷

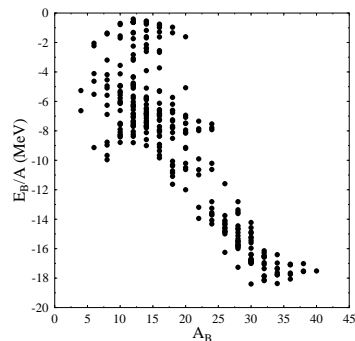


Figure 16: The binding energy per baryon of very light systems of SHM versus the baryon number A .

2.2 Strangelets - Strange Quark Matter

Strange quark matter (SQM) or strangelets are strange clusters containing a large number of delocalized quarks ($u\dots u$, $d\dots d$, $s\dots s$), in multi-quark droplets. Multi-quark states consisting only of u- and d-quarks have masses considerably larger than ordinary nuclei.

Droplets of SQM, which would contain approximately the same amount of u-, d- and s-quarks (strangelets, strange multi-quark clusters), might also be denser than ordinary nuclei. They might exist as long-lived exotic isomers of nuclear matter inside strange neutron stars.

Speculations on the stability of strangelets are based on the following observations:

1. The (weak) decay of a s-quark into a d-quark could be suppressed or forbidden because the lowest single particle states are occupied (Pauli-blocking, analogous to the MEMO case discussed above).
2. The strange quark mass can be lower than the Fermi energy of the u- or d-quark in such a dense quark droplet. Opening a new flavour degree of freedom therefore tends to lower the Fermi energy and hence also the mass per baryon of the strangelet (see Fig. 17), maybe even below the proton mass.

SQM may then appear as a nearly neutral state ($Q \approx u+d+s = \frac{2}{3}e - \frac{1}{3}e - \frac{1}{3}e = 0$).

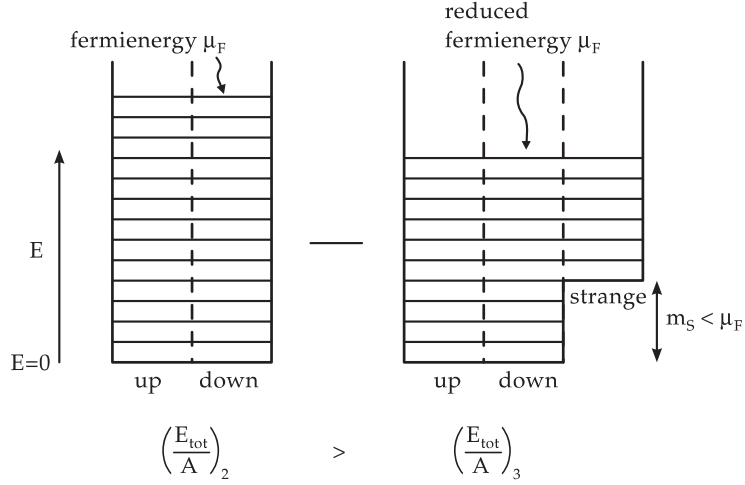


Figure 17: Schematic illustration of the energy levels inside a multi-quark bag with two versus three flavours.

Cold Infinite Quark Matter

Quark matter in *bulk* is often described by an equation of state of interacting quarks to first order in $\alpha_c = g^2/16\pi$ ^{10,11}

$$\begin{aligned}
 \Omega_i(m_i, \mu_i) = & \\
 & -\frac{1}{4\pi^2} \left(\mu_i(\mu_i^2 - m_i^2)^{1/2}(\mu_i^2 - \frac{5}{2}m_i^2) + \frac{3}{2}m_i^4 \ln \frac{\mu_i + (\mu_i^2 - m_i^2)^{1/2}}{m_i} \right. \\
 & \left. - \frac{8}{\pi} \alpha_c \left[3 \left(\mu_i(\mu_i^2 - m_i^2)^{1/2} - m_i^2 \ln \frac{\mu_i + (\mu_i^2 - m_i^2)^{1/2}}{m_i} \right)^2 - 2(\mu_i^2 - m_i^2) \right] \right). \quad (9)
 \end{aligned}$$

Here m_i and μ_i denote the (current) mass and the chemical potential, respectively, of the quark flavour $i=u,d,s$. For the total potential the vacuum excitation energy BV has to be added. It corresponds to the energy difference between the ‘false’, perturbative vacuum inside the ‘bag’ and the true vacuum on the outside

$$\Omega(\mu_q, \mu_s; m_s; \alpha_c) = \sum_{i=u,d,s} \Omega_i(m_i, \mu_i) + BV. \quad (10)$$

From this expression (10) the energy per baryon in the groundstate can be readily obtained. The derivative of E/A with respect to the baryon density is zero if the system is at zero pressure. In Fig. 18 the resulting groundstates are shown for $\alpha_c = 0$ and different bag-parameters a function of the strangeness fraction f_s . The energy per baryon of the corresponding hyperonic matter (taken from the RMF model 1) is also drawn. The tangent construction shown proves that for a given strangeness fraction the separation of a normal and a highly strange subsystem might be energetically favorable as compared to the mixture. Therefore it is energetically advantageous to accumulate the strangeness in the quark phase!

This picture is to big !

Figure 18: The tangent construction at $T = 0$. For a given strangeness fraction f_s the specific energy E/A is lowest for a two-phase mixture of quark and hadronic matter. Drawn are the masses of non-interacting quark matter for different bag parameters and $m_s = 150$ MeV (QGP) and those of infinite hadronic matter in the RMFT model 1 (full line) and model 2 (dashed)²⁹.

Binding Energy per Baryon

The stability of strangelets depends (in the bag model) strongly on the model parameters B and α_c , but also on the baryon number A . Fig. 19 shows the binding energy per baryon as a function of baryon number. Note that this model predicts even with the most optimistic parameter set absolutely stable strangelets only for $A > 25$. All light strangelets ($A < 25$) are found to be metastable, i.e. they will decay, possibly with typical weak interaction decay

times, $\tau \sim 10^{-10} s$.

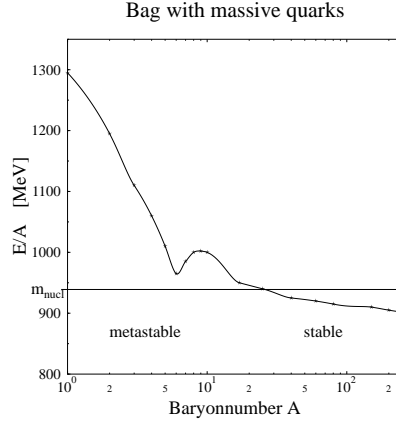


Figure 19: Binding energy per baryon as a function of baryon number. The curve has a local minimum at $A_B=6$, bag constant $B^{1/4}=145$ MeV, $m_s=150$ MeV and $f_s=1.0$ ^{12,13}.

Experiments geared to proof the (non)existence of strangelets therefore should clearly cover such short lifetimes. Unfortunately, this is hard due to the large background of charged hadrons at the target in violent events with high multiplicities. To date all experiments concentrate on long flight-path (to minimize background) and large masses¹⁴, although our prediction is that only metastable strange clusters with \sim cm flight path seem to have a chance of being created. Coalescence calculations of clusters show that high masses are suppressed with a penalty factor of $\exp(-A(m - \mu)/T)$, hence the formation of (even unstable), $A > 20$ hyperclusters seems to be highly unlikely.

Equations of State of Infinite Strangelets

Let us examine now the phase diagram of a hadronic resonance gas in equilibrium with the strange quark matter equation of state derived above. Fig. 20 shows the $\rho_B - T$ plane for a fixed strangeness fraction of $f_s = 0.1$ and $B^{1/4} = 180$ MeV. Even for low temperatures and baryon densities $\rho_B \approx \rho_0$ this simple model predicts the coexistence of a hadron- and a QGP-phase.

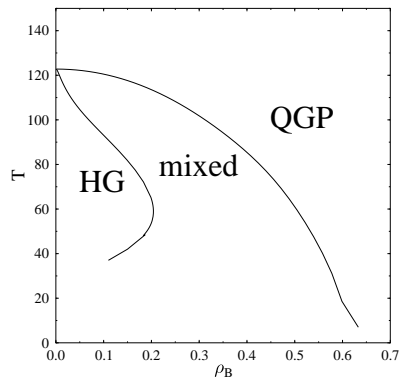


Figure 20: Phase diagram of a hadron gas and infinite quark matter ($B^{1/4} = 180\text{MeV}$) for fixed $f_s = 0.1$.

This illustrates that the thermodynamical properties of a strange system can indeed be strange! Calculations of QGP signals should therefore take this finite net-strangeness degree of freedom into account.

3 Production of Strange Matter in Heavy Ion Collisions

After discussing the possible structure and stability of hyperonclusters and strangelets, let us turn now to possible mechanisms for their creation. Leaving aside (for the moment) astrophysical processes (early universe, supernova, neutron stars), only relativistic, central heavy ion collisions offer events with sufficiently large strangeness production (up to several hundred $s\bar{s}$ pairs per event) to search for multi s (and multi \bar{s} !) clusters. Since the distribution in the phase space of strange and nonstrange particles, is decisive for predictions of hypercluster-probabilities, let us first study the general single particle distributions in central reactions.

3.1 Baryon Dynamics in Heavy Ion Collisions

Dynamics in a Microscopic Model

Fig. 21 exhibits the baryon rapidity distribution as predicted by various models for heavy ion collisions. ATILA¹⁵ and FRITIOF 1.7¹⁶ (not in the picture)

predict no stopping at SPS(CERN). They predict nearly a baryon-free midrapidity already at SPS. This is ruled out by the new CERN data, which rather support predictions based on the RQMD model¹⁷. Fig. 23 shows the scaled final rapidity distribution $\frac{dN}{d(Y/Y_P)}$ (where Y_P is the initial mean rapidity of the projectile) for the system Pb+Pb, $b < 3\text{fm}$, at 200 and 1000 MeV calculated with QMD¹⁸ and the corresponding reaction at 160 GeV calculated with RQMD (histogram). And also FRITIOF 7.02 version¹⁹ yields stopping at SPS! Furthermore, even in very central collisions of lead on lead at $s^{1/2} = 6.5 \text{ TeV}$, there might be some net-baryon density at midrapidity. This is shown in Fig. 22, where the event-averaged rapidity densities of net-baryons, hyperons and anti-hyperons are depicted for the LHC, using FRITIOF 7.02. Even gross features of the baryon dynamics are not yet understood.

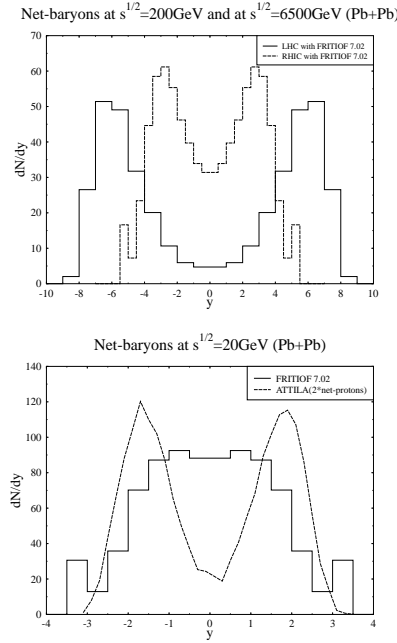


Figure 21: Net-baryon rapidity distribution of very central Pb + Pb collisions at SPS, RHIC, LHC calculated with FRITIOF 7.02. The midrapidity region is even at LHC not baryon-free.

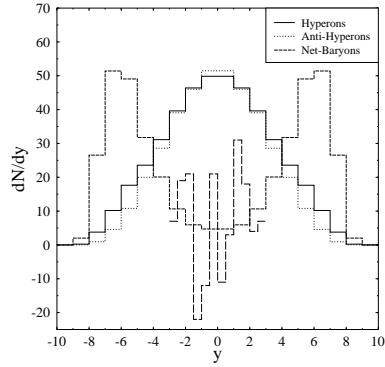


Figure 22: The (anti-)hyperon rapidity distribution of very central Pb + Pb collisions at $s^{1/2} = 6500$ AGeV, and mean net-baryon distribution at midrapidity as compared with a single event calculated with FRITIOF 7.02.

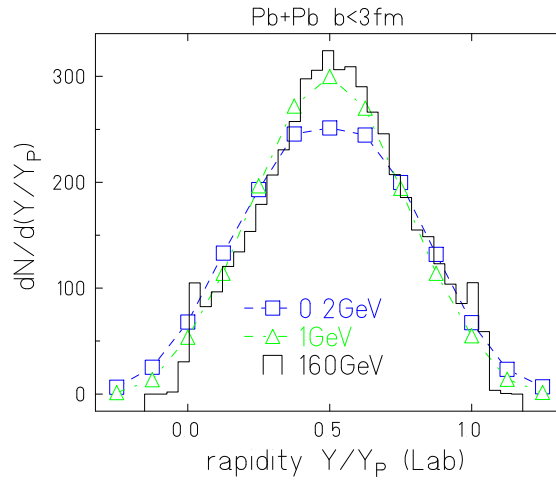


Figure 23: Scaled rapidity distribution for the system Pb+Pb $b < 3$ fm for 200 MeV, 1 GeV and 160 GeV incident energy.²⁰

Local Fluctuations

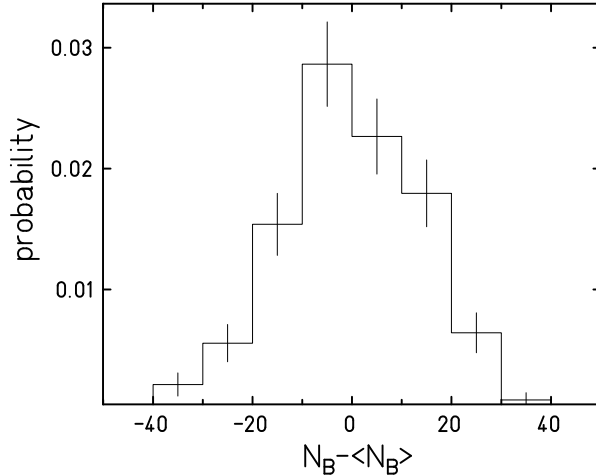


Figure 24: Probability distribution for net-baryon number fluctuations at mid-rapidity within bins of one unit of rapidity width, calculated with FRITIOF 7.02 for the Pb + Pb system at $s^{1/2} = 6500$ AGeV

To estimate the fluctuations possible in heavy-ion collisions at the LHC, let us consider a recent Pb+Pb calculation performed at $s^{1/2} = 6500$ AGeV with FRITIOF 7.02. The probability distribution for non zero net-baryon number fluctuations at midrapidity is plotted in Fig. 24 within bins of one unit of rapidity width. This probability is defined for single events, and shows rapidity density deviations from the average value $\langle dN/dy \rangle$. Bins between $-3 < y < 3$ have been taken into account. The probability for fluctuations $N_B - \langle N_B \rangle$ being larger than ± 20 is about 15 %. The asymmetry of the histogram results from the fact that fluctuations may be different for positive and negative deviations around a non zero average rapidity density. This aspect is visible clearly in the dN/dy of a randomly selected single event as drawn (for the mid-rapidity region) in Fig. 22.

Keep in mind that the microscopic models used here ignore possible effects that could change significantly the number of produced strange particles in heavy ion collisions, e.g. the string-string-interactions to be discussed now.

3.2 Medium Effects

String-String Interaction

Fig. 25 depicts the multiplicities of different produced particles at LHC as function of the string-tension κ .

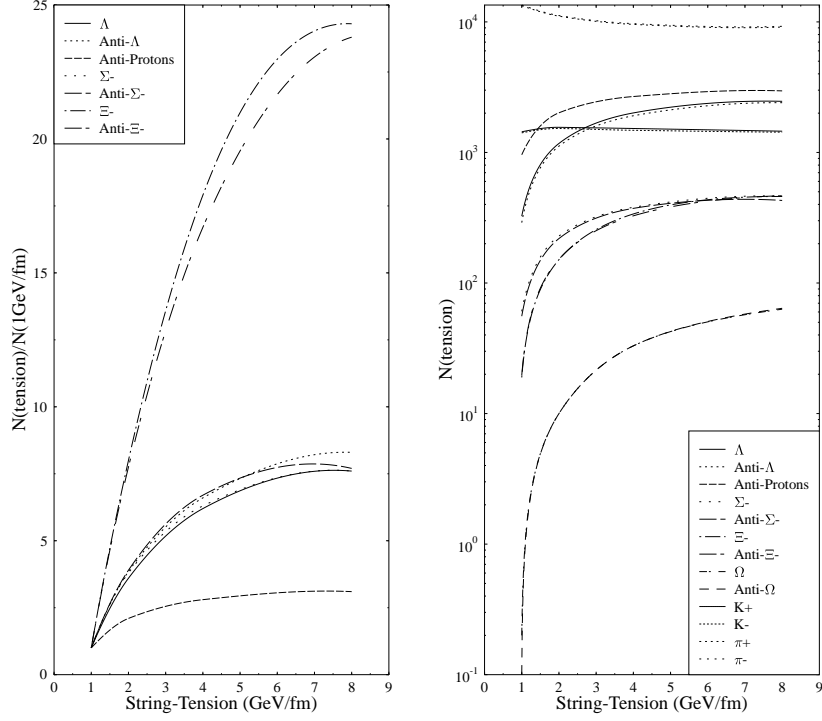


Figure 25: The multiplicities of different particles in very central Pb + Pb collisions at 6500 AGeV as function of the string-tension calculated with FRITIOF 7.02.

The number of produced baryons increases with κ while the number of mesons decreases. This can be read off the formula:

$$|M|^2 \propto \exp\left(-\frac{\pi m^2}{\kappa}\right) . \quad (11)$$

Here $|M|^2$ is the probability to produce a parton-antiparton pair with the mass m for a string-tension κ . This formula is motivated by the Schwinger-

formalism²¹ for pair-production in an infinite electric field. The string-tension of 1 GeV/fm (no interaction) leads to a suppression of the heavier strange quarks (s) and diquarks (di), as compared to up (u) and down (d) quarks. The following input is used in our calculations :

$$\frac{|M|_u^2}{|M|_d^2} : \frac{|M|_s^2}{|M|_u^2} : \frac{|M|_s^2}{|M|_d^2} : \frac{|M|_{di}^2}{|M|_u^2} = 1 : 1 : 0.3 : 0.1,$$

corresponding to $m_s = 280$ GeV.

A higher string-tension, e.g. 2 GeV/fm yields the suppression factors :

$$\frac{|M|_u^2}{|M|_d^2} : \frac{|M|_s^2}{|M|_u^2} : \frac{|M|_s^2}{|M|_d^2} : \frac{|M|_{di}^2}{|M|_u^2} = 1 : 1 : 0.55 : 0.32$$

Such enhanced string tensions may effectively simulate string-string interactions.

Another source for the enhanced production of heavy quarks in such reactions can be a reduced effective quark mass. When a string fragments in a dense medium, an effective constituent quark mass of say, $m = 0.5m_0$ results in the same suppression factor as a fourfold increase of the string-tension, $\kappa = 4$ GeV/fm. The constituent quark masses could be possibly reduced in the vicinity of a chiral phase transition.

Reduction of the constituent quark masses

The relativistic meson-field models, which, at high temperature, qualitatively simulate chiral behaviour of the nuclear matter (see next paragraph), exhibit a transition into a phase of massless baryons²². Including hyperons and YY -interaction⁷ at $\mu \approx 0$, the densities for all (anti)-baryon species considered are of the order of ρ_0 near the critical temperature.²³ Thus, the fraction of (anti)-strange quarks increases drastically. Several hundred (anti)-baryons, most of them (anti)-hyperons, may then fill the hot midrapidity region (with net baryon number ≈ 0). Fig. 26 shows this phase transition for (anti-)nucleons and (anti-)hyperons at small μ . Below $T_C \approx 170$ MeV the anti-baryons are strongly suppressed due to the positive baryochemical potential. The (anti-)hyperons suffer an additional suppression because of their higher mass. Above T_C all effective masses are small and the relative yields in the medium are dictated by the isospin degeneracy, thus favouring (anti-)hyperonic matter.

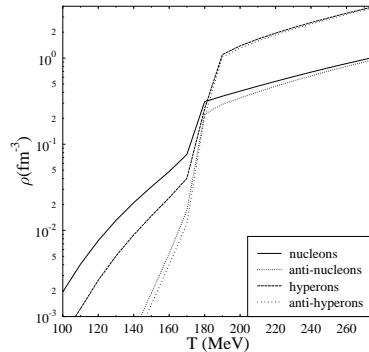


Figure 26: Densities of (anti-)nucleons and (anti-)hyperons as functions of temperature for fixed $\mu_q = 100$ MeV and strangeness fraction $f_s = 0$, calculated with the relativistic meson-baryon field theory (RMF model 2).

Similar results can be found with a chiral $SU(3) \times SU(3)$ Lagrangean²⁴. Now that we have demonstrated that a wealth of in-medium effects can increase drastically the single particle (strange)baryon density, let us consider the clustering of the hyperons by using a phase space coalescence model.

3.3 Clustering of Hypermatter

The generalized phase space coalescence model has been applied successfully to light (p,n)clusters and anticlusters. Fig. 27 shows a calculation of antideuteron²⁵ which exhibit a characteristic phase space structure due to strong absorption. However, the strange quarks or the hyperons should be more localized in phase space. Thinking in terms of a coalescence picture for producing exotic multistrange clusters, such an early increase in the net strangeness content, whether a QGP has been formed or not, should affect the production probability of these clusters.

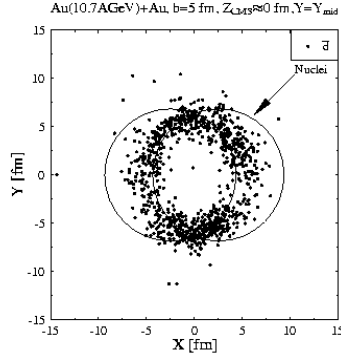


Figure 27: Antimatter is only emitted from the surface of the hot and dense fireball, created in heavy ion collisions ²⁵.

Microscopic models (Venus, RQMD, FRITIOF,...) do not include the production of light exotic nuclei dynamically. Cluster formation can be added after the strong freeze-out i.e. after the last strong interaction of the particle. The cluster formation probability can be calculated by projecting the baryon pair phasespace on the cluster wave function via the Wigner-function method as described in ^{26,27,28}. The yield of exotic two-particle-clusters is given by

$$dN_{\text{Cluster}} = \text{const} \left\langle \sum_{i,j} \rho_{\text{Cluster}}^{\text{w}}(\Delta\vec{R}, \Delta\vec{P}) \right\rangle d^3(p_{i_{B,Y}} + p_{j_{B,Y}}).$$

The Wigner-transformed wavefunction of the cluster is denoted by $\rho_{\text{Cluster}}^{\text{w}}$. The sum goes over all baryons and hyperons, whose relative distance ($\Delta\vec{R}$) and relative momentum ($\Delta\vec{P}$) are calculated in their rest frame at the time after both nucleons have ceased to interact. The constant accounts for the statistical spin and isospin projection on the desired state. The calculation of higher mass fragments is straight forward by exchanging the two particle cluster wavefunction with a n-body harmonic oscillator wavefunction, summing up over all possible baryon combinations. RQMD predicts three $\Lambda\Lambda$ - and one $\Sigma^-\Sigma^-$ -cluster in 100 Pb+Pb collisions at SPS. An additional strangeness distillation occurs when there is a first order phase transition from a quark matter state to a hadron fluid.

3.4 Strangelet Distillation

Consider a hadronizing QGP-droplet with net-strangeness zero surrounded by a layer of hadron gas which continuously evaporates hadrons (they undergo the freeze-out). Assume the two phases to be in perfect mechanical, chemical and thermal equilibrium. Now, rapid kaon emission leads to a finite *net* strangeness of the expanding system¹². This scenario is visualized in Figs. 28 and 29(left). This results in an enhancement of the *s*-quark abundance in the quark phase. Prompt kaon (and, of course, also pion) emission cools the quark phase, which then condenses into metastable or stable droplets of SQM.

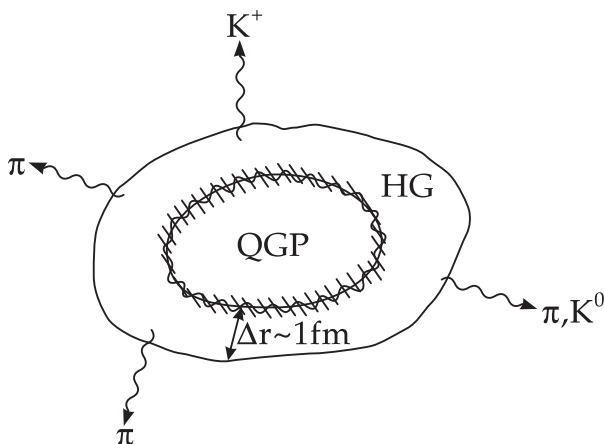


Figure 28: Hadron gas surrounds the QGP at the phase transition. Particles evaporate from the hadronic region. New hadrons emerge out of the plasma by hadronization.

Distillation at High Baryon Densities

Fig. 29 (right) shows the properties of a strangelet in its time evolution for two different bag constants and a moderate initial specific entropy of $S/A = 25$. The ratio of the quarkchemical potential and the temperature $|\mu|/T$ is directly related to the entropy per baryon number via

$$\left(\frac{S}{|A_B|}\right)^{\text{QGP}} \approx \frac{37}{15}\pi^2 \left(\frac{|\mu|}{T}\right)^{-1}. \quad (12)$$

Therefore, we deal with rather high net baryon densities in the system. Strangelets can survive if they are allowed to cool down. In any scenario, strangeness is accumulated in the quark phase. From this it seems misleading

to extract "temperatures" and "chemical potentials" from detected particle ratios, since their abundances reflect time integrated values, not a specific break-up μ/T combination. The rates of the emitted hadrons are dictated by the (strange) chemical potentials which are strongly time dependent.

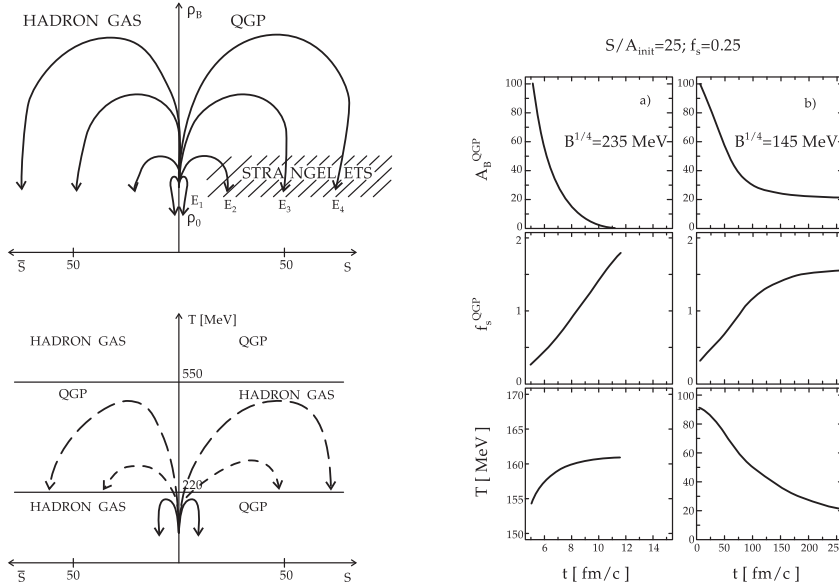


Figure 29: Left : The fountain of strangeness production²⁹. The distillation of strangeness is more effective for high baryon densities. Right¹² : a) Baryon number, strangeness content and temperature of the quark glob during complete hadronization as a function of time for a very large bag constant $B^{1/4} = 235$ MeV. The initial values are an initial baryon content of $A_B(t_0) = 100$, an entropy per baryon ratio of $S/A(t_0) = 25$ and an initial net strangeness fraction of $f_s(t_0) = 0.25$. Note the strong increase of the strangeness content with time. b) The same situation as in a), however, for a small bag constant $B^{1/4} = 145$ MeV, when a strangelet is distilled. One observes a strong decrease in the evolving temperature.

Fig. 30 illustrates that the different species are radiated off after different times: e. g. the lambdas stem from the very last stage while the kaons are emitted very early.

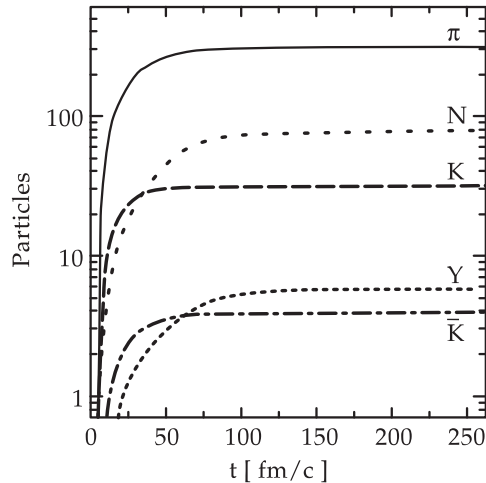


Figure 30: The number of emitted particles are shown versus time in a situation, when a strangelet is distilled. The conditions are the same as in the previous figure b), however, no initial net strangeness is assumed.¹²

Distillation at low μ/T

At collider energies, the midrapidity region is expected to be characterized by low net-baryon densities. How can one expect to create stable strangelets with baryon density of $\rho > \rho_0$?

Fig. 31 illustrates the increase of baryon density in the plasma droplet as an inherent feature of the dynamics of the phase transition. This result originates from the fact that the baryon number in the quark-gluon phase is carried by quarks with $m_q \ll T_C$, while the baryon density in the hadron phase is suppressed by a Boltzmann factor $\exp(-m_{\text{baryon}}/T_C)$ ($m_{\text{baryon}} \gg T_C$). A very tiny excess of initial net-baryon number will suffice to generate regions of very high density $\rho_B > \rho_0$! The very low initial μ/T corresponds to high values of the initial specific entropy.

Fig. 32 shows the evolution of the two-phase system for $S/A^{\text{init}} = 200$, $f_s^{\text{init}} = 0$ and for a bag constant $B^{1/4} = 160$ MeV in the plane of the strangeness fraction vs. the baryon density. The baryon density increases by more than one order of magnitude! Correspondingly, the chemical potential rises as drastically during the evolution, namely from $\mu^i = 16$ MeV to $\mu^f > 200$ MeV.

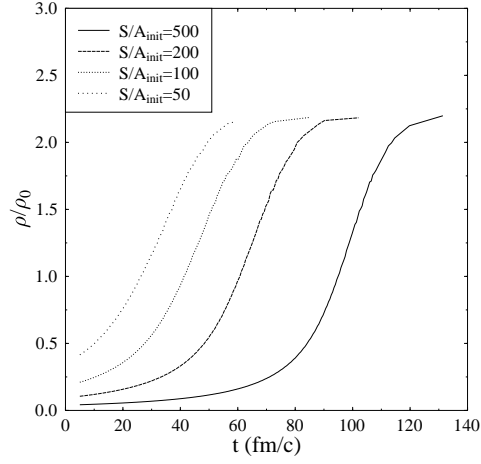


Figure 31: Time evolution of the net baryon density of a QGP droplet. The initial conditions are $f_s^{\text{init}} = 0$ and $A_B^{\text{init}} = 30$. The bag constant is $B^{1/4} = 160$ MeV.²³

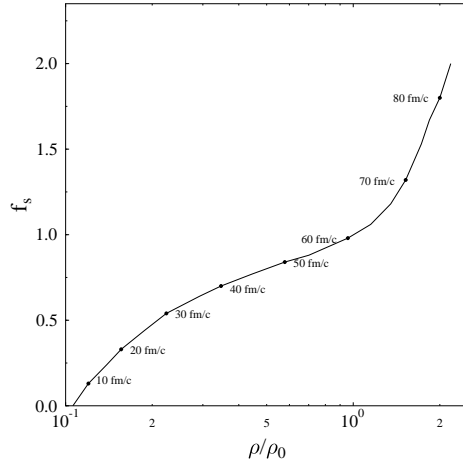


Figure 32: Evolution of a QGP droplet with baryon number $A_B^{\text{init}} = 30$ for $S/A^{\text{init}} = 200$ and $f_s^{\text{init}} = 0$. The bag constant is $B^{1/4} = 160$ MeV. Shown is the baryon density and the corresponding strangeness fraction.²³

The strangeness separation mechanism³⁰ drives the chemical potential of the strange quarks from $\mu_s^i = 0$ up to $\mu_s^f \approx 400$ MeV. Thus, the thermodynamical and chemical properties during the time evolution differ drastically from the initial values! Low initial chemical potentials do not hinder the creation of strangelets with high μ .

4 Experiments - On the Search of Strange Matter

4.1 Present experiments – the search for absolutely stable strange matter

The key for the detection of strange (quark) matter is the predicted low charge-to-mass ratio. In contrast to normal nuclei with $Z/A = 0.5$, strange matter should have charge-to-mass ratios as small as $\pm 1 : 10$ or $\pm 1 : 20$.

Strangelets and MEMOs in flight are practically indistinguishable from each other experimentally, but they can be unambiguously separated from normal (anti-)matter.

Searches for strange quark matter in Au+Au collisions at the AGS have been performed³¹, but only for a small acceptance close to zero degrees, for charge-to-mass ratios higher than 1:25.

Large acceptance data will be gathered at Brookhaven with the E864 detector³².

At CERN a search for strange matter has been started using a 500 m long setup. First lead on lead data have yielded upper limits of 10^{-7} per event for strange matter.

The sensitivity of the experiments can be increased by several orders of magnitude. However, all these experiments are unable to observe metastable hyperclusters due to the required lifetimes $\tau \gg 10^{-10}$ s. This is dictated by the long flight path in these experiments.

4.2 Future experiment – searching for shortlived strange matter

The lifetime of a MEMO or a strangelet could be similar to the Λ lifetime ($\sim 10^{-10}$ s). Thus, a short flight path, open geometry detector will be needed to discover these objects. If a produced strangelet is absolutely stable with respect to strong interaction, the only energetically possible decay mode is the weak leptonic decay ($s \rightarrow d, Q \rightarrow Q' + e + \bar{\nu}$), which will transmute the strangelet to the strangelet minimum energy. The time-scale for this weak process has been estimated to be $\sim 10^{-4}$ s¹⁰.

But in case that strangelets or MEMOs are metastable (this is the case in a much wider range of parameters) the weak conversion rate $u + s \leftrightarrow u + d$ for almost cold SQM can be calculated³³. It is $\sim 10^{-6} - 10^{-7}$ s. Subsequent weak

decay processes, as described here, ‘heat’ up the droplet (on a scale of a few MeV). The droplet may be cooled by γ -radiation or by nucleon emission. Both processes compete with each other. Still, the lifetime issue is not settled.

5 Conclusion

Strange-baryon yields can go up by orders of magnitude at T_c due to changes in the string tension or the effective mass at a phase transition (e.g. in chiral models). The clustering probability for strange matter should then increase correspondingly.

For strong decays, the short lifetime could not allow to see strangelets and MEMOs directly.

However, measurements of Hanbury-Brown-Twiss-correlations between two or more hyperons can be applied to prove the (non)existence of strange matter. To achieve sensitivity in detectors for two (or more) strange particles per event, the singles rate must be high, though.

Negatively charged hyperclusters (e.g. $Z = -2, f_s = 2$) might exist with positive baryon number. Their experimental signature in magnets should be similar to that of anti-nuclei ($\overline{\text{He}}$), however, they would **not** show the additional annihilation energy of antinuclei in calorimeters.

Baryochemical potentials may turn out to be nonzero (even at y_{cm}) at colliders, with $\mu/T \sim 1$. The event by event rapidity dependence of π, p, \bar{p}, Y and \bar{Y} should be measured to clarify this issue.

This could also reveal fluctuations of the (strange) net-baryon number.

Even the small, but finite stopping power of baryons at LHC can provide phase space regions with $\mu > T$.

The baryon distillery mechanism drives the chemical potential from $\mu_B^i, \mu_s^i \approx 0$ to $\mu_B^{Qf} \gg \mu_B^i, \mu_S^{Qf} \sim \mu_B^{Qf}$. If such a first order phase transition exists, the quark phase charges up rapidly with strangeness. The system will therefore not stay in the $\rho, T(f_s=0)$ plane, but will follow a complicated three-dimensional path in the space (ρ, T, f_s) . This can affect severely many of the QGP signals discussed to date. Unfortunately almost nobody has yet undertaken such a study. Finite f_s -values change the phase structure completely! The coexistence region then ranges possibly down to $\rho_B \approx \rho_0$ and $T \approx 20\text{MeV}$.

The bag term is crucial for the time evolution of the QGP. For $B^{1/4} \geq 180$ MeV the lifetime of the mixed phase can be large! Multi- Λ -evaporation at the end of the hadronization will signal by HBT- (or multi-correlation-)analysis the decaying short-lived ”strangelet”. For $B^{1/4} < 180$ MeV metastable strangelets ($Z \approx -2$?) can be formed and might be detected directly.

References

1. W. Greiner, Int. Journ. of Phys. E (January 1996) 1
2. S. Hofmann (Darmstadt, GSI). GSI-95-25, Apr. 1995. 8pp. Contributed to 15th Nuclear Physics Divisional Conference on Low Energy Nuclear Dynamics, St. Petersburg, Russia, 18-22 Apr 1995.
3. Particle Data Group, Phys. Rev, D50, (1994) 1173
4. J. Schaffner, C.B. Dover, A. Gal, D.J. Millener, C. Greiner, H. Stöcker: Ann. of Phys. (N.Y.) **235**, (1994) 35
5. J. Boguta, S. Bohrman Phys. Lett. 102B (1981) 93
6. J. Schaffner, C. Greiner, H. Stöcker: Phys. Rev. C**46**, (1992) 322
7. J. Schaffner, C.B. Dover, A. Gal, C. Greiner, H. Stöcker: Phys. Rev. Lett. **71**, (1993) 1328
8. C.E. Crien et al., Il Nuovo Cimento 102A (1989) 727
9. R.H. Dalitz, F.R.S., D.H. Davies, P.H. Fowler, F.R.S, A. Montwill, J. Pniewski, J.A. Zakrewski: Proc. Roy. Soc. Lond. A**426**, (1989) 1
10. S. A. Chin and A. K. Kerman, Phys. Rev. Lett. **43**, (1979) 1292
11. J. D. Bjorken and L. D. McLerran, Phys. Rev. D**20**, (1979) 2353
12. C. Greiner and H. Stöcker, Phys. Rev. D**44**, 3517 (1991)
13. P. Papazoglou, M. Bleicher, A. Jahns, J. Schaffner, H. Stöcker, C. Greiner Intern. Symposium of Strangeness and Quark Matter Sept. 1.-5.1994 World Scientific (1995) 206
14. NEWMASS Collaboration (NA52), CERN/SPSLC **268**, March 13, (1992)
15. M. Gyulassy, private communication
16. B. Nilsson-Almqvist and E. Stenlund, *Comput. Phys. Comm.* **43** (1987) 387
17. H. Sorge, H. Stöcker, W. Greiner Ann. Phys. (USA) **192** (1989) 266; Nucl. Phys. A**498** (1989) 567c; Z. f. Phys. C**47** (1990) 629
18. J. Aichelin, H. Stöcker Phys. Lett. B176 (1989) 14
19. H. Pi, *Comput. Phys. Comm.* **71** (1992) 173-192
20. Ch. Hartnack et al. Nucl. Phys. A**538** (1992) 53c
21. J. Schwinger; Phys. Rev. **82** (1951) 664
22. J. Theis, G. Graebner, G. Buchwald, J. Maruhn, W. Greiner, H. Stöcker, J. Polonyi, Phys. Rev. D**28** (1983) 2286
23. C. Spieles, L. Gerland, H. Stöcker, C. Greiner, C. Kuhn, J. P. Coffin, subm. to Phys. Rev. Lett. (1995)
24. P. Papazoglou et al., to be published
25. M. Bleicher *et al.*, nucl-th/9506009, Phys. Lett. B in print (1995)
26. R. Mattiello, A. Jahns, H. Sorge, H. Stöcker, W. Greiner, *Phys. Rev. Lett.* **74** (1995) 2180

27. M. Gyulassy, K. Frankel, E.A. Remler, *Nucl. Phys.* **A402** (1983) 596
28. E.A. Remler and A.P.Sathe, *Ann. Phys.* **91** (1975) 295
29. A. Diener, diploma thesis Frankfurt/a. M. (1994)
30. C. Greiner, P. Koch and H. Stöcker, *Phys. Rev. Lett.* **58**, (1987) 1825;
C. Greiner, D. H. Rischke, H. Stöcker and P. Koch, *Phys. Rev. D* **38**,
(1988) 2797
31. H. J. Crawford and C. H. Greiner, *Scientific American*, January, 1994
vol. 270 no.1
32. J. Sandweiss, Proc. of the Pre-Conference Workshop, Quark Matter '95,
Monterey, California, USA (1995), UCRL-ID-121571, p. 205
33. P. Koch, *Nucl. Phys.* **B24B**, (1991) 255